NORMAL TEMPERATURE MECHANICAL PROPERTIES OF 6082 ALUMINIUM ALLOY
AS A FUNCTION OF TEMPERING TEMPERATURE:
EXPERIMENTAL AND NUMERICAL APPROACH

Abdelmalek ELHADI */** , **Salah AMROUNE */**** , **Amin HOUARI ***** , **Madani KOUDER ******

*Mechanical Department, Faculty of Technology, University of Msila, Msila, Algeria
**Materials and Structural Mechanics Laboratory (LMMS). University of M'sila, M'sila, Algeria
***Faculty of Technology, M'hamed Bougara, University, Boumerdes 35000, Algeria
****Laboratoire de Matériaux, et Mécanique des Structures (LMMS), Université SBA. Sidi Bel Abesse, Algérie

abdelmalek.elhadi@univ-msila.dz, salah.amroune@univ-msila.dz, houari.latif2016@gmail.com, koumad10@yahoo.fr

Abstract: Our study involved a combination of practical experiments and numerical simulations using the Abaqus computational software. The main aim was to enhance our understanding of the mechanical characteristics exhibited by 6082 aluminium alloy when exposed to tensile forces. To achieve this, we produced 18 samples of standardized dimensions utilizing a parallel lathe. These samples then underwent a thermal treatment comprising a solution treatment, water quenching and various tempering procedures at different temperatures (280°C, 240°C, 200°C, 160°C and 120°C), resulting in a range of hardness levels. To obtain the experimental results, we conducted tensile tests on a specialized machine, which were subsequently supplemented with numerical analyses. By adopting this approach, we gained valuable insights into the behaviour of aluminium alloy 6082, specifically regarding its mechanical properties such as hardness, tensile strength, elongation and necking coefficient. This newfound knowledge holds potential significance in the realm of designing and optimizing aluminium structures that operate within high-temperature environments.

Key words: 6082 Aluminium alloy, quenching and tempering, hardness, tensile strength

1. INTRODUCTION

Aluminium alloys have been the subject of much research and scientific progress. Their importance in industry lies in their characteristic properties such as low densities. They are two to four times lower than that of steels. They are widely applied, especially in the aeronautical, automotive and shipbuilding industries (1). The mechanical properties of Al–Mg–Si alloys can be improved by including the additional elements or by applying appropriate heat treatments such as solution heat treatment, quenching and ageing treatment (2). 6082 Aluminium alloy (ISO name: AlSiMg07) has favourable mechanical properties, good corrosion resistance and good mechanical strength of the order of 320 MPa in the T6 state (3). The presence of silicon and copper reduces thermal expansion, while magnesium increases it (4, 5). This alloy is mainly used in the transport and structural engineering industry, such as in bridges, cranes, frameworks, transport aircraft and transport ships. The mechanical properties of this alloy such as hardness and breaking strength are improved by heat treatments (6-8).

Researchers have studied the effect of temperature on the mechanical properties of aluminium alloy in tensile tests on cylindrical specimens accompanied by numerical simulation. Terena et al (9) conducted experimental and numerical analyses on the drawing efficiency of quenching aluminium alloy 6082. Validation of the theoretical evaluation was performed by superimposing the graph of the triaxiality ratio of stress versus strain plastic and the

failure envelope graph of the 60820 quenching aluminium alloy for a zero seam parameter. The numerical simulation gave the ratio of triaxiality of the stresses compared with the correlation of the plastic deformations. In order to define the constituent material model and the rupture envelope, experimental determinations and numerical simulations of plane stress and plane strain specimens were carried out (tensile, shear and compression tests for various samples). The simulation results were compared with experimental observations. Recent works have revealed important data on this matter, such as Clausen et al. (10), who targeted the dependence of fracture on strain rate, triaxiality and temperature, or Field et al. (11), who studied various materials submitted to high rate shock. Mean stress was proven to play an important role in the fracture of metals by Bao and Wierzbicki (12). Their numerical simulations with the cut-off value in fracture loci successfully captured the main features observed in tensile tests under hydrostatic pressure. Furthermore, Wierzbicki et al. (12) have shown the advantage of working with plane stress.

This work studies the influence of heat treatment on the mechanical properties of alloy 6082 before and after the treatment. To do this, the specimens are organized into 6 series of 3 samples each; therefore a total of 18 samples are tested. It should be noted that the experimental results obtained are processed and analysed by the Abaqus software in order to make a comparison between the experimental and numerical results.

sciendo

Abdelmalek Elhadi, Salah Amroune, Amin Houari, Madani Kouder
Normal Temperature Mechanical Properties of 6082 Aluminium Alloy as a Function of Tempering Temperature: Experimental and Numerical Approach

DOI 10.2478/ama-2024-0042

2. MATERIALS AND METHODS

The tensile specimen material used is 6082 aluminium alloy. The results of the spectroscopic chemical analysis (wt%) of the alloy are shown in Tab. 1.

Tab. 1. The chemical composition of the material (wt%)

Mg	Si	Cu	Fe	Mn	Zn	Ni	Cr
1.20	0.85	0.71	0.78	0.56	0.40	0.17	0.07

The geometric shape and the dimensions (in mm) of the specimen chosen (according to the ISO 6892-1 standard) are represented in Fig. 1.
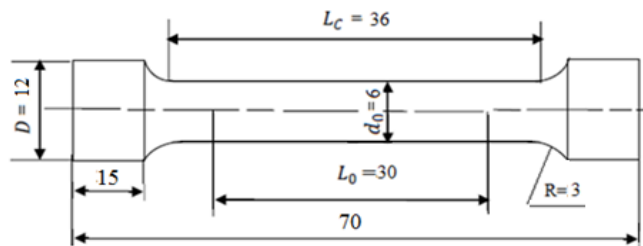
Fig. 1. Tensile specimen used

The average hardness of the material in the delivered state is 118 HV. The type of heat treatment applied to the specimens is the structural hardening treatment as shown in Fig. 2:

− Solid solution: Heating at a high temperature of 540°C for 30 min to put in the solid solution (a mixture of pure substances forming a homogeneous solid) the greatest possible number of soluble hardening elements.
− Rapid cooling: Water is often used as a quenching medium to keep the solid solution supersaturated (13).
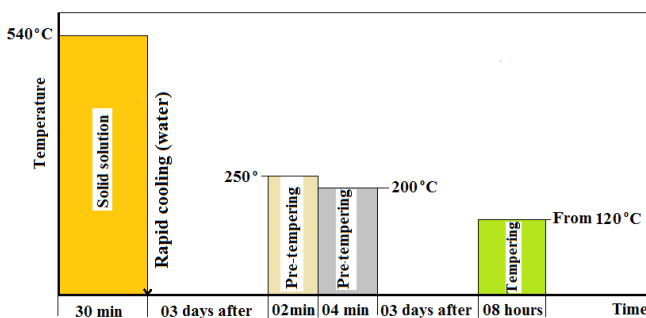

Fig. 2. Structural hardening treatment of AL6082

Industrially, tempering cannot always be carried out immediately after quenching. Different effective remedies have been found, particularly in the case of A-SG alloys. This can be done for example as follows:

Pre-tempering in two stages: Pre-tempering for 2 min at 250°C + 4 min at 200°C (3 days after quenching). The short pre-tempering time allows for 1 week in which the time between quenching and tempering has minimal effect on the mechanical properties and prevents natural ageing.

The tempering time of AL6082 is between 8 and 10 h.

Tempering for 8 h: Applied 3 days after pre-tempering at 280°C, 240°C, 200°C, 160°C and 120°C.

Fig. 3 shows two specimens, one before heat treatment (Fig. 3a) and the other after solution treatment and quenching (Fig. 3b).
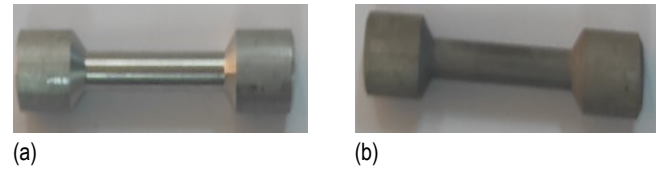

(a)   (b)

Fig. 3. Tensile specimens: (a) Before heat treatment; (b) After heat treatment

The average value of the hardness of the 6082 aluminium alloy used after quenching is 103 HV (decrease in hardness compared with the untreated material [118 HV]).

It is a hydraulically driven vertical column test apparatus (Fig. 4). The maximum pulling force can reach 50 KN in both directions. The strain rate used in tensile tests 0.2 mm/min.

Fig. 4. Tensile machine WP 310

3. CONSTITUTIVE MODEL OF THE MATERIAL AL6082-T6

The aluminium specimens were modelled as an elastoplastic material by Johnson–Cook plasticity and the damage criterion introduced in the ABAQUS calculation code was used to develop numerical simulations in order to study the structural response of the metal. This criterion provides a satisfactory description of the behaviour of metal and alloys, since it takes into account large strains, high strain rates and temperature-dependent viscoplasticity. For this purpose, the temperature factor in the aluminium alloy was taken into account. We therefore used the Johnson–Cook material model to determine the equivalent stress in the following form:

$$\sigma_{JC} = [A + B(\bar{\varepsilon}^p)^n]\left[1 + C.ln\left(\overline{\bar{\varepsilon}^p}/\overline{\dot{\varepsilon}_0^p}\right)\right]\left[1 - \left(\frac{\theta_w - \theta_0}{\theta_m - \theta_0}\right)^m\right] \quad (1)$$

Where A, B, C, m and n are five materials constants. A is the yield strength, B is the strength coefficient, C is the strain rate coefficient, n is the strain hardening coefficient and m is the thermal softening coefficient. σ_{JC} is the flow stress, ε is the plastic strain, . $\bar{\varepsilon}^p$ is the plastic strain rate, . $\dot{\varepsilon}_0^p$ is the reference plastic strain rate, θ_0 is the temperature of the workpiece material, θ_w is the reference temperature, and θ_m is the melting temperature of

the materials. Many criteria have been developed to predict the damage of metallic materials in the case of loadings. They rely on either of the maximum strain conditions for damage initiation. Damage in the Johnson–Cook material model is predicted using the following cumulative damage law:

$$W = \sum \frac{\Delta \bar{\varepsilon}^p}{\bar{\varepsilon}_f^p} \qquad (2)$$

where $\Delta \bar{\varepsilon}^p$ is the accumulated increment of equivalent plastic strain during an integration step, W is the damage parameter for fracture initiation when it is equal to 1 $\bar{\varepsilon}_f^p$ as the deformation equivalent to rupture, deduced as follows:

$$\bar{\varepsilon}_f^p = \left[D_1 + D_2 \exp\left(D_3 \frac{P}{\sigma_{JC}} \right) \right] \left[1 + D_4 . \ln\left(\overline{\dot{\varepsilon}^p} / \bar{\dot{\varepsilon}}_0^p \right) \right] \left[1 - D_5 \left(\frac{T_w - T_0}{T_m - T_0} \right)^m \right] \qquad (3)$$

$\frac{P}{\sigma_{JC}}$ is the mean stress normalized by the equivalent stress, and parameters D_1, D_2, D_3, D_4 and D_5 are constants. The evolutions of the damage are defined by the energy condition to create new free surfaces (Eq. 2). The choice of the energy approach is often governed by the size of the finite elements.

$$G_f = \int_{\bar{\varepsilon}_0^{pl}}^{\bar{\varepsilon}_f^{pl}} L \sigma_y d\bar{\varepsilon}^{pl} \qquad (4)$$

Thus, following the initiation of the damage, the variable of damage increases according to the following equation:

$$D = \frac{L d \bar{\varepsilon}^{pl}}{\bar{u}_f^{pl}} \qquad (5)$$

$\frac{P}{\sigma_{JC}}$ the plastic displacement equivalent to fracture is calculated as in the following equation:

$$\bar{u}_f^{pl} = \frac{2 G_f}{\sigma_{y0}} \qquad (6)$$

where σ_{y0} is the elastic limit of the material, G_f is the fracture energy and L is the characteristic of the finite element.

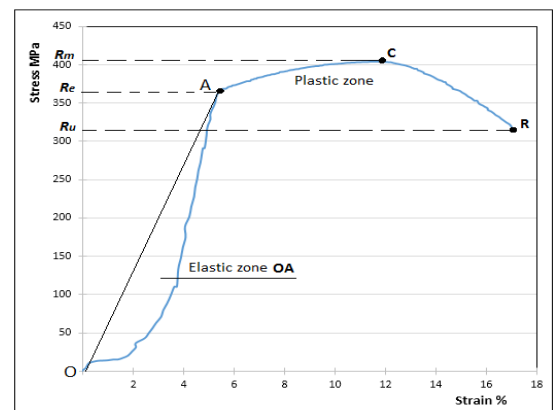**Tab. 2.** Johnson–Cook constitutive model constants for AL 6082-T6

Al6082-T6	Value
A (MPa)	360
B (MPa)	249
N	0.62
C	0.008
Tm (°C)	582
T (°C)	25
M	0.6122
D1 [17]	0.0164
D2 [17]	2.245
D3 [17]	−2.798
D4	−0.284
D5	−2.342

Tab. 2. Johnson–Cook constant and static tensile strength for AL 6082-T6 of the strain rate used in tensile tests 0.2 mm/min.
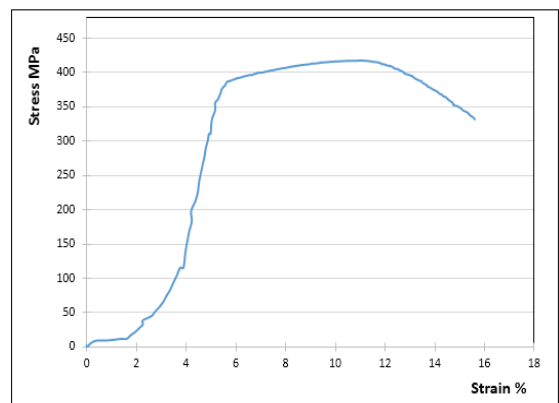
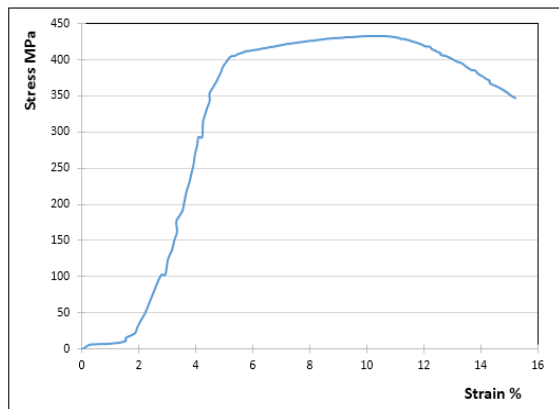# 4. RESULTS

4.1. Tensile behaviour of material

The specimens used in a tensile test are prepared according to international standards. The stress–strain curve obtained from the tensile test of the material used is shown in Fig. 5. All the curves have the same appearance and reflect the mechanical behaviour of the material in tension (14, 15). We take as an example Fig. 5a, where the stress–strain curve starts with the elastic strain or the material, following Hooke's law which expresses the linearity between stress and strain. With increase in the tensile load, the material enters the plastic zone (permanent deformation) up to a maximum load which is expressed in relation to the initial section of the specimen tensile strength Rm. After that, the deformation is concentrated in one area, where there is necking (throttling) and then the rupture of the specimen.
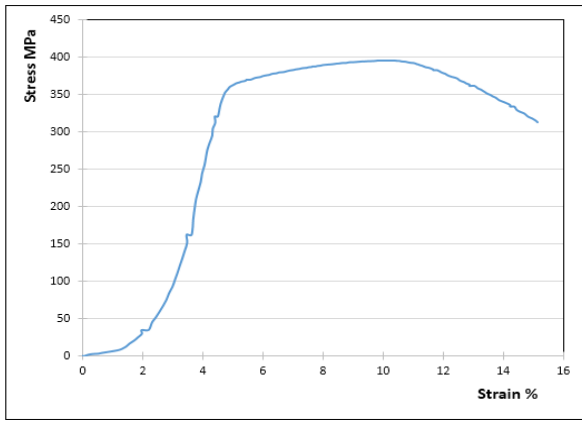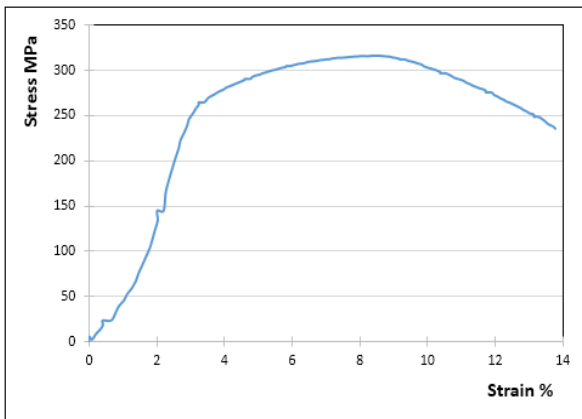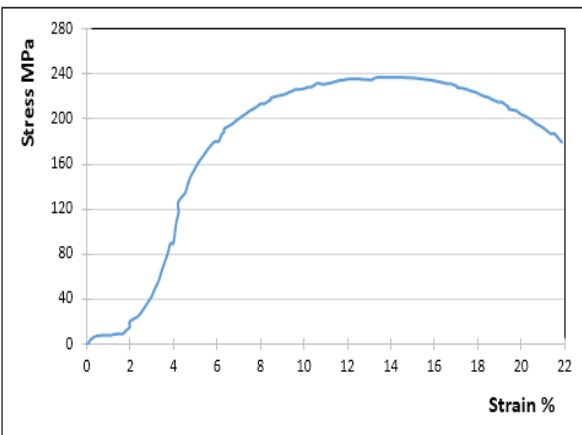

(a)

(b)

(c)

Abdelmalek Elhadi, Salah Amroune, Amin Houari, Madani Kouder
Normal Temperature Mechanical Properties of 6082 Aluminium Alloy as a Function of Tempering Temperature: Experimental and Numerical Approach

DOI 10.2478/ama-2024-0042

(d)

(e)

(f)

Fig. 5. Stress–strain curves of 6082 Aluminium alloy: (a) Untreated; Tempering temperature: (b) 120°C; (c) 160°C; (d) 200°C; (e) 240°C; (f) 280°C

4.2. Variation of hardness as a function of tempering temperature

The evolution of the average hardness HV as a function of tempering temperature is shown in Fig. 6. This figure shows a decrease in hardness values with increasing tempering temperature.
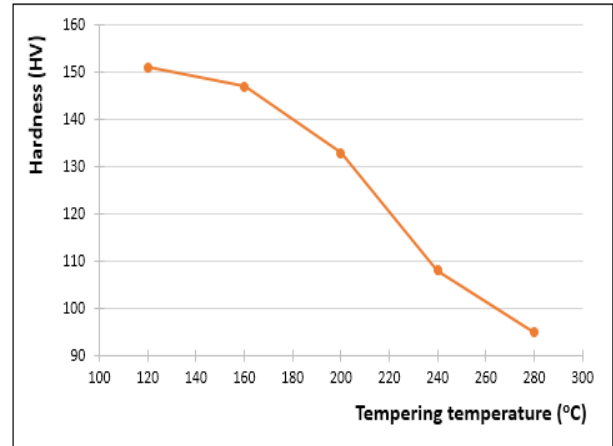

Fig. 6. Evolution of the hardness as a function of tempering temperature

4.3. Evolution of the tensile strength Rm as a function of tempering temperature

The evolution of the tensile strength as a function of the tempering temperature is shown in Fig. 7. It can be seen that the tensile strength for the material is maximum at the tempering temperature of 160°C (422 MPa) and minimum at the tempering temperature of 280°C (214 MPa).
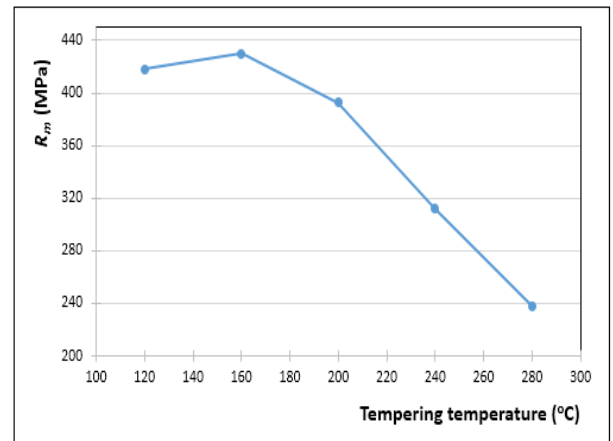

Fig. 7. Evolution in tensile strength as a function of tempering treatment

4.4. Variation in elongation A% as a function of tempering temperature

The percent elongation of the specimen (*A%*) is the ultimate elongation. It is determined by the formula:

$$A\% = 100\frac{Lu-Lo}{Lo} \tag{7}$$

with L_o: initial length and L_u: length after rupture.

Fig. 8 shows that the elongation values of the material are close to the tempering temperature of 120–280°C. On the contrary, the elongation is maximum at the tempering temperature of 280°C (7.92%).
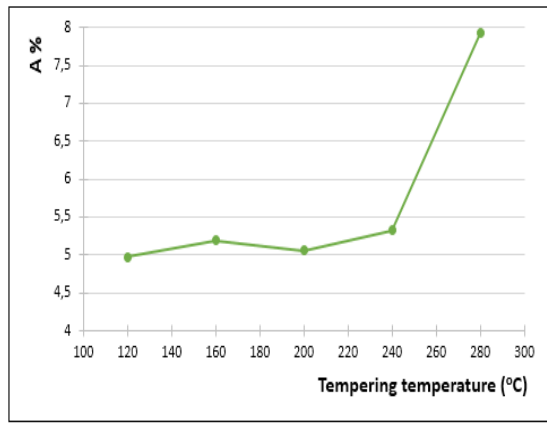
Fig. 8. Evolution of elongation as a function of tempering temperature

4.5. Variation of the coefficient of necking Z% as a function of tempering temperature

The percent necking coefficient of the specimen (Z%) is determined by the formula:

$$Z\% = 100\,\frac{So - Su}{So} \tag{8}$$

with S_o: initial section and S_u: section after rupture.

Fig. 9 presents the results obtained from the coefficient of necking Z% as a function of tempering temperature. The increase in the tempering temperature leads to an increase in the coefficient of necking.
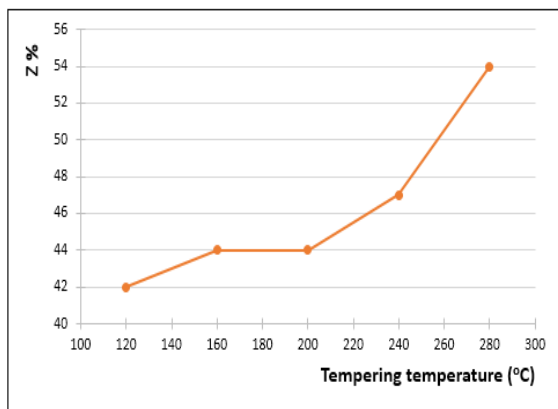

Fig. 9. Evolution of the coefficient of necking as a function of tempering temperature

5. DISCUSSION

For the alloy quenched and tempered to 280°C, the hardness decreased (95 HV), when compared with the hardness value of the alloy in the as-delivered condition (untreated: 110 HV). This is attributed to the effect of quenching, which prevents the reformation of precipitates and therefore a softening of the alloy. The tempering effect (artificial ageing) of 6082 aluminium alloy shows an increase in hardness and mechanical strength, but a slight decrease in elongation with the decrease in tempering temperature. This phenomenon is due to structural hardening by precipitation, which is the decomposition of a supersaturated solid solution (homogeneous phase having at least two constituents) into a mixture of two phases of different composition: intermetallic iron

IMF and Mg2Si (16). From the above, it can be said that the optimum tempering temperature is at 160°C, due to its best characteristics given for the alloy; in other words, a fairly large hardness, resistance to rupture important and improved ductility, which is necessary for the operating conditions of materials in general.

A comparison of the experimental and numerical curves shows that numerical results are consistent with the experimental results. They exhibit similar trends with an almost constant difference for all the tensile tests, as shown in Figs. 10–15.
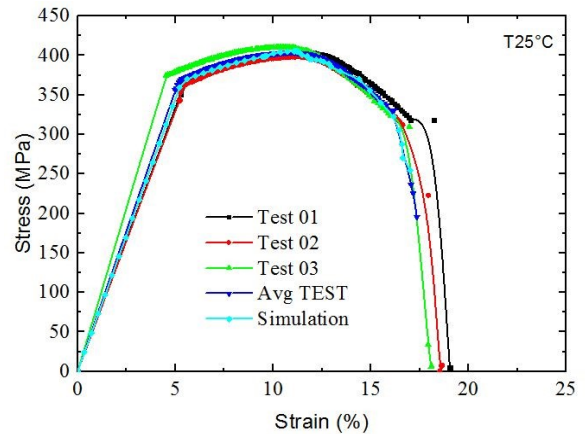

Fig. 10. Experimental and numerical curves of the evolution of stress–strain as a function of the tempering temperature of the material in the delivery state T = 25°C
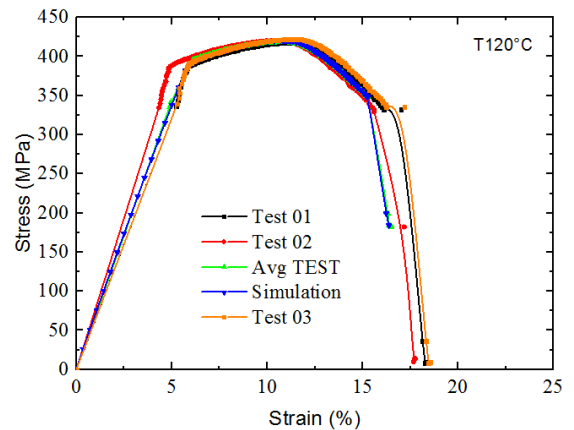

Fig. 11. Experimental and numerical curves of the evolution of stress-strain as a function of the tempering temperature (120°C)
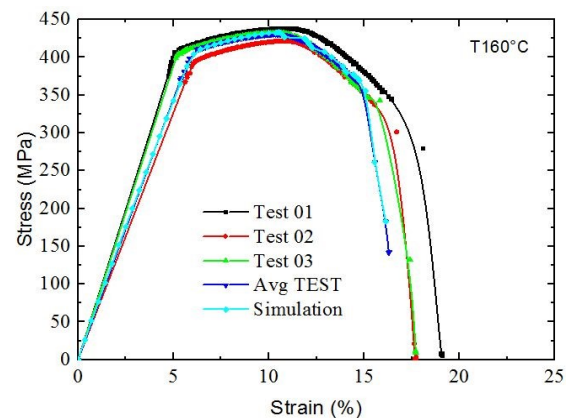

Fig. 12. Experimental and numerical curves of the evolution of stress–strain as a function of the tempering temperature (160°C)

Abdelmalek Elhadi, Salah Amroune, Amin Houari, Madani Kouder
Normal Temperature Mechanical Properties of 6082 Aluminium Alloy as a Function of Tempering Temperature: Experimental and Numerical Approach
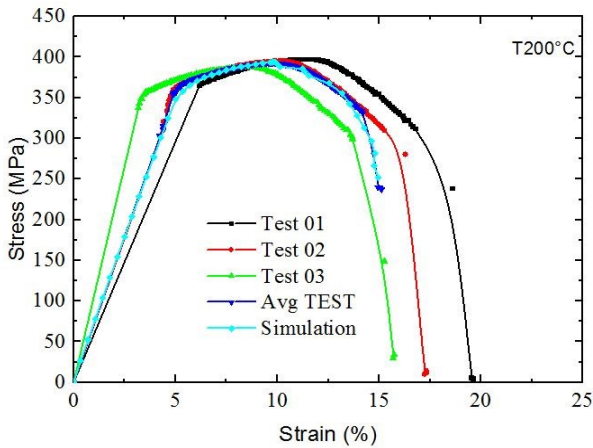
DOI 10.2478/ama-2024-0042

Fig. 13. Experimental and numerical curves of the evolution stress-strain as a function of the tempering temperature (200°C)
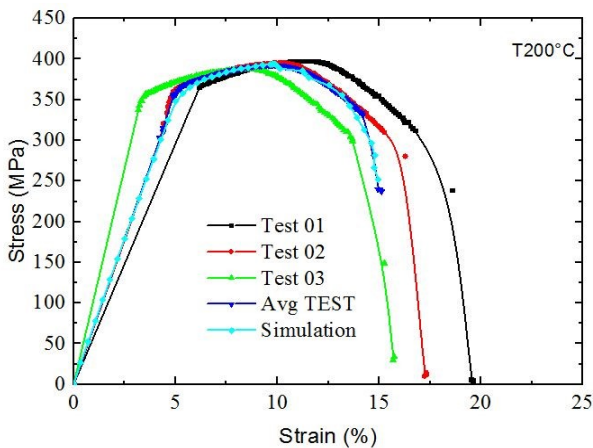

Fig. 14. Experimental and numerical curves of the evolution stress-strain as a function of the tempering temperature (240°C)
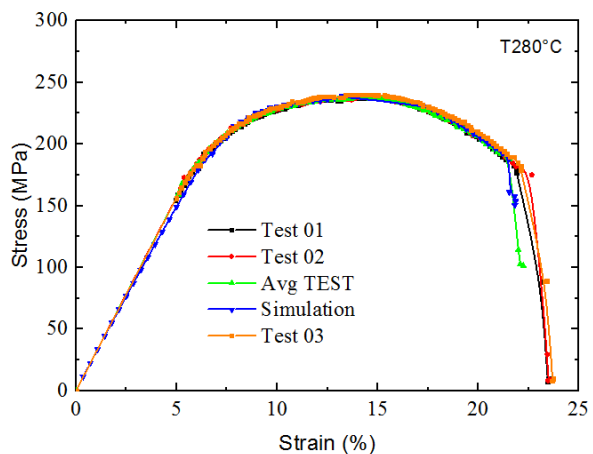

Fig. 15. Experimental and numerical curves of the evolution stress–strain as a function of the tempering temperature (280°C)

To verify the accuracy of the numerical model, tensile tests were conducted using Abaqus at temperatures ranging from 280°C, 240°C, 200°C, 160°C to 120°C. The experimental curves and the numerical load–displacement curves are presented in Figs. 10–15, where their shapes are fairly consistent, and the corresponding ultimate failure models are also reasonably well identified for the different temperatures. To illustrate, let us con-

sider the specimens treated at temperatures of 160°C and 280°C. The experimental results reveal average mechanical characteristics, with the rupture stress recorded at 430.19 MPa and 237.96 MPa, and the corresponding rupture strains at 10.58% and 13.92%, respectively. On the contrary, in the numerical simulation, the rupture stress is estimated to be around 432.89 MPa and 238.84 MPa, while the rupture strains are approximately 10.35% and 13.21%. This leads to small deviations, with errors of approximately 0.62% and 0.37% for the stress values, and 2.17% and 5.10% for the strain values. Furthermore, it is noteworthy that these errors remain within acceptable limits. The comparison between the experimental and simulated data shows a strong agreement, with discrepancies not exceeding 6% for all the cases studied. This outcome emphasises the reliability and accuracy of the simulation results. Similarly, the comparison for the remaining cases exhibits a consistent pattern. The error between the experimental and simulation results for both stress and strain measurements remains below 6%. This demonstrates a high level of agreement and confirms the fidelity of the simulation model. Overall, the analysis of the experimental and simulation data demonstrates that the numerical model accurately captures the mechanical behaviour of the specimens. The results consistently align with the experimental findings, confirming the validity and effectiveness of the simulation approach. Such close agreement between the two datasets provides confidence in the reliability of the numerical simulations and their ability to predict the mechanical response of the specimens under different conditions and temperatures.

Tab. 3 indicates the different results obtained experimentally and numerically of the tensile strength as a function of the tempering temperature.

Tab. 3. Different results experimentally and numerically of the tensile strength

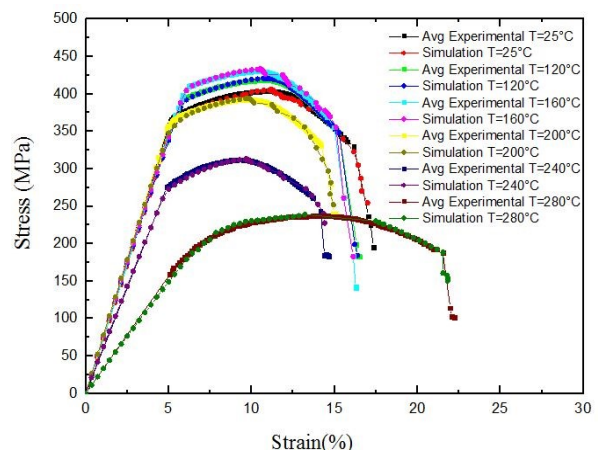| Tempering temperature	R_m (MPa) moy	Simulation R_m	Error %
25	403.94	404	0.01
120	418	420.8	0.67
160	430	432.5	0.58
200	393	392.5	0.13
240	312	313	0.32
280	237.96	238.5	0.23

Fig. 16. Experimental and numerical stress–strain curves from tensile tests

Fig. 16 groups together all the experimental and numerical stress–strain curves for all the tensile tests carried out.

Tab. 4 indicates the different results obtained experimentally, numerically and error of the stress and strain as a function of the tempering temperature. The experimental values obtained represent the average of three tests recorded for each series of specimens at different temperatures.

The comprehensive examination of this table unmistakably reveals that the disparity between the experimental and simulation results, be it for stress or strain, is well within the acceptable range.

Tab. 4. Different results obtained experimentally, numerically and error of the stress and strain as a function of the tempering temperature

Tempering temperature (°C)	Exp σ (MPa)moy	Sim σ (MPa)	Error E1 (%)	Exp δ (%)	Sim δ (%)	Error E2 (%)
25	403.94	405.36	0.36	10.92	11.25	3.02
120	418.76	420.87	0.51	10.75	11.04	2.69
160	430.19	432.89	0.62	10.58	10.35	2.17
200	392.532	393.98	0.37	9.78	10.01	2.35
240	412.21	313.05	0.26	9.30	9.69	4.19
280	237.96	238.84	0.37	13.92	13.21	5.10

6. CONCLUSION

The aluminium alloy 6082 plays a crucial role in the industry, and its mechanical properties can be enhanced through suitable heat treatments to enable optimal usage conditions. This study has yielded the following conclusions:

− Quenching the 6082 aluminium alloy resulted in a reduction in its hardness, with an average value of 103 HV after quenching, compared with the initial hardness of the material before quenching, which was 118 HV.

− Tempering above a certain temperature may decrease the hardness of the alloy less than the hardness as delivered, for example, tempering at 280°C reduced the average hardness to 95 HV.

− A decrease in the tempering temperature results in an increase in hardness. The tempering temperature 120°C is required to obtain high hardness 151 HV.

− Heat treatments can modify the mechanical properties of aluminium alloy 6082 in various ways.

− A decrease in the tempering temperature leads to an increase in mechanical strength and a slight decrease in elongation.

− The tensile strength for the material is maximum at the tempering temperature of 160°C (422 MPa) and minimum at tempering temperature 280°C (214 MPa).

− The experimental and simulation outcomes, whether it be for stress or strain, are comfortably within the acceptable range, with an error margin of no more than 6%. These results emphasize a significant alignment between the two sets of data and provide confirmation of the simulation's precision.

REFERENCES

1. Narayana GV, Sharma V, V Diwakar, Kumar KS, Prasad R. Fracture behaviour of aluminium alloy 2219–T87 welded plates. Science and technology of welding and joining. 2004;9(2):121-130. https://doi.org/10.1179/1362171104225017035

2. Kang H, Park JY, Choi YS, Cho DH. Influence of the solution and artificial aging treatments on the microstructure and mechanical properties of die-cast Al–Si–Mg alloys. Metals. 2021;12(1):71. https://doi.org/10.3390/met12010071

3. Gabryelczyk A, S Ivanov, Bund A, Lota G. Corrosion of aluminium current collector in lithium-ion batteries: A review. Journal of Energy Storage. 2021;43:103226. https://doi.org/10.1016/j.est.2021.103226

4. Kumar CR, Malarvannan RRR, JaiGanesh V. Role of SiC on Mechanical. Tribological and Thermal Expansion Characteristics of B₄C/Talc-Reinforced Al-6061 Hybrid Composite. Silicon. 2020; 12(6):1491-1500. 10.1007/s12633-019-00243-0

5. Watts SJ, Hill RG, O'Donnell MD, Law RV. Influence of magnesia on the structure and properties of bioactive glasses. Journal of Non-Crystalline Solids. 2010;356(9):517-524. https://doi.org/10.1016/j.jnoncrysol.2009.04.074

6. Prabhu Swamy NR, Ramesh CS, Chandrashekar T. Effect of heat treatment on strength and abrasive wear behaviour of Al6061-SiCp composites. Bulletin of Materials Science. 2010;33(1):49-54. 10.1007/s12034-010-0007-y

7. Aboulkhair NT, Maskery I, Tuck C, Ashcroft I, Everitt NM. The microstructure and mechanical properties of selectively laser melted AlSi10Mg: The effect of a conventional T6-like heat treatment. Materials Science and Engineering: A. 2016;667:139-146. https://doi.org/10.1016/j.msea.2016.04.092

8. Wang LF, Sun J, Yu XL, Shi Y, Zhu XG, Cheng LY, Liang HH, Yan B, Guo LJ. Enhancement in mechanical properties of selectively laser-melted AlSi10Mg aluminum alloys by T6-like heat treatment. Materials Science and Engineering: A. 2018;734:299-310. https://doi.org/10.1016/j.msea.2018.07.103

9. Trană E, Rotariu AN, Lixandru P, Matache LC, Enache C, Zecheru T. Experimental and numerical investigation on 6082 0 temper aluminium alloy cartridge tubes drawing. Journal of Materials Processing Technology. 2015;216:59-70. https://doi.org/10.1016/j.jmatprotec.2014.08.032

10. Clausen AH, Børvik T, Hopperstad OS, Benallal A. Flow and fracture characteristics of aluminium alloy AA5083–H116 as function of strain rate, temperature and triaxiality. Materials Science and Engineering: A. 2004;364(1):260-272. https://doi.org/10.1016/j.msea.2003.08.027

11. Field J E, Walley SM, Proud WG, Goldrein HT, Siviour CR. Review of experimental techniques for high rate deformation and shock studies. International Journal of Impact Engineering. 2004;30(7):725-775. https://doi.org/10.1016/j.ijimpeng.2004.03.005

12. Wierzbicki T, Bao Y, Lee YW, Bai Y. Calibration and evaluation of seven fracture models. International Journal of Mechanical Sciences. 2005;47(4):719-743. https://doi.org/10.1016/j.ijmecsci.2005.03.003

13. Mohamed A, Samuel FH. A review on the heat treatment of Al-Si-Cu/Mg casting alloys. Heat Treatment-Conventional and Novel Applications. 2012;1:55-72. http://dx.doi.org/10.5772/79832

14. Rao D, Huber K, Heerens J, dos Santos JF, Huber N. Asymmetric mechanical properties and tensile behaviour prediction of aluminium alloy 5083 friction stir welding joints. Materials Science and Engineering: A. 2013;565:44-50. https://doi.org/10.1016/j.msea.2012.12.014
15. Kang J, Rao H, Zhang R, Avery K, Su X. Tensile and fatigue behaviour of self-piercing rivets of CFRP to aluminium for automotive application. in IOP Conference Series: Materials Science and Engineering. 2016. IOP Publishing.
16. Hillert M. On theories of growth during discontinuous precipitation. Metallurgical and Materials Transactions B. 1972;3(11):2729-2741. 10.1007/bf02652840

Abdelmalek Elhadi: https://orcid.org/0000-0002-9825-9488

Salah Amroune: https://orcid.org/0000-0002-9565-1935

Amin Houari: https://orcid.org/0009-0004-2617-2182

Kouider Madani: https://orcid.org/0000-0003-3277-1187